

Titre-DMD – A Rapid Constant pH Molecular Dynamics Framework

David J. Reilley,[†] Jian Wang,[‡] Nikolay V. Dokholyan,^{*,§} Anastassia N. Alexandrova^{*,†,||}

[†] Department of Chemistry and Biochemistry, University of California, Los Angeles, Los Angeles, California 90095-1569, United States

[‡] Department of Pharmacology, Department of Biochemistry & Molecular Biology, Penn State University College of Medicine, Hershey, Pennsylvania 17033, United States

[§] Departments of Chemistry and Biomedical Engineering, Pennsylvania State University, University Park, Pennsylvania 16802, United States

^{||} California NanoSystems Institute, Los Angeles, California 90095-1569, United States

KEYWORDS: CpHMD, pK_a , DMD, Dynamics

ABSTRACT: The pH dependence of enzyme fold stability and catalytic activity is a fundamentally dynamic, structural property which is difficult to study. Computational methods, particularly constant pH molecular dynamics (CpHMD), are the best situated tools for this. However, these often struggle with affordable sampling of sufficiently long timescales, accuracy of pK_a prediction, and verification of the structures they generate. We introduce Titre-DMD, an affordable CpHMD method with a protonation state sampler that can be systematically improved, to circumvent these issues. We benchmark the method on a set of proteins with experimentally attested pK_a and on the pH triggered conformational change in a staphylococcal nuclease mutant, a rare experimental study of such behavior. Our results show Titre-DMD to be an effective method to study pH coupled protein dynamics.

Introduction

Solution pH is a chemical property with an immense effect on protein behaviors that are difficult to study at the atomic scale. Peak protein fold stability and catalytic activity are both dependent on an often narrow range of pH . Understanding the sequential and structural underpinning of these preferences contributes to the design and application of enzymes, particularly extremophile enzymes – which would allow for their use in harsher reaction conditions in industrial catalysis,^{1–4} and answers a wide range of questions of medical interest as precise pH regulation is critical for cellular homeostasis.^{5–7} However, this understanding demands atomistic information of fundamentally dynamic phenomena. pH -dependent dynamics is challenging to study experimentally, requiring a combination of techniques like NMR monitored pH -titration, circular dichroism spectroscopy, and X-ray crystallography none of which alone provide the complete picture. This experimental complexity leaves computational investigation⁸ as a critical tool to fill in the gaps.

Successful computational methods that assess pH dependent protein behavior must accurately couple amino acid protonation state change with conformational dynamics. Typically, continuum electrostatic methods describe the protonation states of amino acids, assessing the free energy of protonation and deprotonation events or pK_a . Various solutions to the Poisson-Boltzmann equation can provide this,⁹ especially the generalized Born model.^{10,11} Tools such as UHBD,¹² H++,¹³ and Propka^{14,15} predict the pK_a of amino acid residues in proteins

based on static structures, but can not fully capture pH -dependent dynamic behavior. Molecular dynamics can provide the missing conformational sampling. The combinations of these tools are known as constant pH molecular dynamics (CpHMD); these methods generally use continuum electrostatic methods to model the protonation state changes of amino acids over the course of a molecular dynamics simulation.

The appropriate sampling of pH coupled dynamics is difficult to achieve for all CpHMD methods and challenging to verify. The choice of solvation model is central to sampling and broadly breaks CpHMD methods into two categories. Implicit solvent-based methods offer rapid sampling with the treatment of the surrounding solution as a simple dielectric medium.^{16–19} Explicit solvent based methods can provide greater accuracy through atomistic solvent treatment, but sufficient sampling is difficult to achieve, as both conformational and protonation states need to be sampled. Furthermore, protonation sampling is affected by poor overlap between solvent configurations such that protonation state changes are often immediately rejected. To counter this, many groups have applied λ -dynamics, based off pioneering work by Brooks et al.²⁰ (in turn based on earlier work with other thermodynamic properties in mind),^{21,22} which treats the protonation state of individual amino acid sites as continuous degrees of freedom rather than discrete ones sampled distinctly.^{23–25} Other efforts focus on enhancing/accelerating conformational sampling through GPU processing²⁶ or replica exchange.^{27,28} Ultimately,

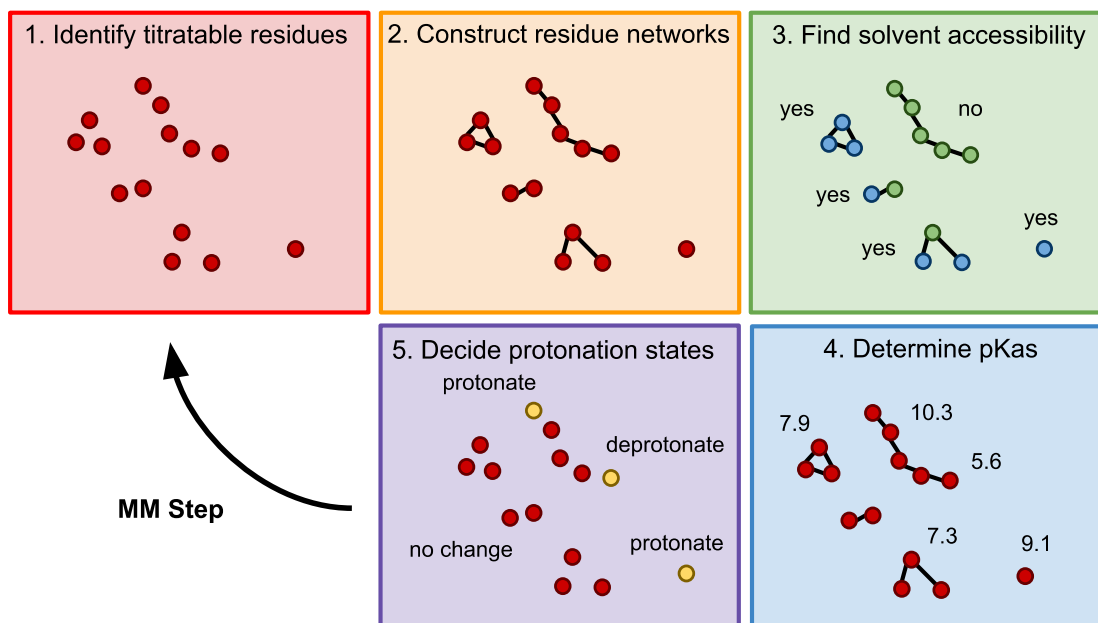


Figure 1: Schematic of the Titr-feature algorithm. This runs between short DMD (or any molecular mechanics) simulations to assign discrete protonation states.

regardless of solvation, one struggle for all CpHMD methods is verification of the ensemble of conformational and protonation states they generate, due to paucity of complementary experimental results. Most methods instead benchmark through more plentiful indirect evidence, such as reconstruction of titration curves or estimation of experimental pK_a values. It is unclear if the generated ensemble of structures is physically meaningful by comparison to those metrics alone.

We present here Titr-DMD as an undemanding method for the investigation of pH dependent protein behavior. Our method dynamically updates the protonation states of a discrete molecular dynamics (DMD) simulation²⁹⁻³¹ using pK_a predicted for instantaneous structures along its trajectory as probabilities. In the current implementation Titr-DMD uses pK_a values generated through the semi-empirical continuum electrostatics method Propka, but is not restricted to this tool. DMD’s square-well potentials (reducing the number of necessary calculations) and implicit solvation provide rapid conformational sampling on limited resources, while a Monte Carlo algorithm confers extensive protonation state sampling. Our program is highly modular for easy modification as better approaches for instantaneous pK_a prediction develop. We benchmark Titr-DMD on both its ability to calculate ensemble pK_a compared to experiment and on its ability to capture the pH dependent conformational change found experimentally in staphylococcal nuclease (SNase).³² While other CpHMD methods have studied pH -coupled protein dynamics,^{33,34} including in the SNase system,³⁵ recapturing protein dynamics is not a common benchmark for method development.

Theory and Methods

Titr-DMD method. This method combines rapid DMD²⁹ conformational sampling with a custom algorithm to resolve protonation based on Propka3.1¹⁴ pK_a predictions. Simulations are performed iteratively, alternating between a short DMD simulation and a titration (Titr)-feature that discretely assigns protonation states. The algorithm for the Titr-feature itself comprises five steps: (1) titratable residues are identified, (2) contact networks are constructed from these

residues, (3) the solvent accessibility of each network is determined, (4) the probability of protonation state change is determined for each network or residue, (5) protonation state changes are determined by a Monte Carlo scheme (Figure 1).

The intervals between protonation state reassessment are run just long enough so that protonation and deprotonation are equilibrated over the DMD simulation timescale. As isolated proton transfer events, like many individual reaction steps in proteins,³⁶ generally occur on the femtosecond to picosecond timescale,³⁷ 200 DMD steps (which is ~ 10 ps) suffices, a comfortable separation of 1-3 orders of magnitude. This allows for both the consistent and meaningful application of theory, discussed more thoroughly throughout this section, and extensive sampling of a system’s potential protonation states. A higher reassessment frequency is therefore unnecessary and computationally expensive; while additional time spent on the Titr-feature itself is minimal, a higher frequency requires more, shorter DMD simulations and thus more time overhead during the program initialization.

Selection of titratable residues is based on their solution pK_a values. The amino acids aspartate, glutamate, histidine, cysteine, tyrosine, lysine, and arginine are the only ones to have side-chain solution pK_a values in the physiological range of pH 1-13 and so are the only ones considered. While significant shifts in pK_a often occur when an amino acid is part of a protein, all other residues have side-chain pK_a that fall far enough out of this range to be largely irrelevant in the vast majority of systems. For the same reason, only the first protonation/deprotonation event is considered for the included amino acids; states like doubly deprotonated lysine or doubly protonated glutamine are inaccessible. The C-terminal carboxylate and N-terminal amine could be titrated as well, but are not currently implemented due to missing DMD potentials for their less preferred states.

Contact networks are constructed on the basis of the proximity of titratable residues. First, interacting pairs of residues are identified based on their (de)protonatable heteroatoms that are within a certain cutoff distance, r_p , of each other. This pro-

tonation contact distance r_p is selected as 3.5 Å to be consistent with the DMD definition of a long hydrogen bond. Each thus defined network represents a series of residues close enough that in the timeframe of the DMD phase of the Titr-DMD simulation the proton exchange is equilibrated between them and lies firmly under thermodynamic control.

Solvent accessibility of each residue contact network is determined in a manner consistent with Propka, which defines a specific residue as buried or exposed based on its contact number, $w(N)$. $w(N)$ is determined by the number of heavy atoms, N , within 15 Å of the residue's charge center according to

$$w(N) = \begin{cases} 0 & \text{if } N \leq N_{\min} \\ \frac{N - N_{\min}}{N_{\max} - N_{\min}} & \text{if } N_{\min} < N < N_{\max} \\ 1 & \text{if } N \geq N_{\max} \end{cases}$$

The residue is thus 0% buried if $N \leq 280$ (N_{\min}) and 100% buried if $N \geq 560$ (N_{\max}).¹⁴ In the Titr-feature, a network is considered solvent accessible if any residue in it is below a certain cutoff. As proton exchange is equilibrated within a network, so long as one residue is solvent accessible the rest of the network can freely exchange protons with solvent. The best value of this solvent access cutoff is a parameter in the model and in general might be system dependent. We find that the most appropriate value for the solvent access cutoff could range from 45% to 75% and matters most in systems with important, frequently buried residues. Alternative approaches to the solvent access cutoff are also possible. We discuss this fully in the future development of Titr-DMD section and within our test system simulations.

The probability of a protonation state change is assessed for each titratable residue based on instantaneous pK_a and the residue network information. In this implementation Propka3.1 is used for pK_a prediction, based on the latest structure from the preceding DMD trajectory. The protonation state change probability is then assessed for each residue. It is calculated differently depending on whether the residue is in a solvent accessible or inaccessible network. For a solvent accessible network the probability is based on the pH of the solution with which the residue can freely exchange protons (solvent is treated implicitly in DMD). This probability is based off the Henderson-Hasselbash equation

$$pH = pK_a + \log\left(\frac{[D]}{[P]}\right)$$

where $[D]$ is the concentration of the deprotonated state and $[P]$ is the concentration of the protonated state. From this, the probability of adopting the protonated state, P_p , can be defined as

$$P_p = \frac{[P]}{[P] + [D]} = \frac{10^{pK_a - pH}}{1 + 10^{pK_a - pH}}$$

In the solvent inaccessible case, only the titratable protons already present in the network can be exchanged. The probabilities of protonation state changes for the residues in this contact network are thus coupled; protonation state changes must be determined for the whole network at once, rather than residue by residue. This requires full enumeration of all proton configurations across the network. The preference of a proton to localize on any individual residue is determined by its pK_a , but with comparison to the competing residues in the network rather than the solution pH . To calculate this, let R be the set of

all residues in a network and n be the number of titratable protons in that network. Let $T|n(R)$ be the set of all possible proton configurations S, Q, \dots such that $T|n(R) = \{S \in T(R) : |S| = n\}$. Then for every $S \in T|n(R)$ the probability of adopting that proton configuration is

$$P_C(R, S) = \frac{\prod_{s \in S} 10^{pK_a(s)}}{\sum_{Q \in T|n(R)} \prod_{q \in Q} 10^{pK_a(q)}}$$

The weighting term for each proton configuration is the product of 10 raised to the pK_a of each residue that holds a proton in that state ($s \in S, q \in Q, \dots$). This equation is used to calculate the probability of each possible configuration.

Finally, protonation state changes are decided discretely by a Monte-Carlo approach based on the probabilities generated for each network. As with the probabilities, this differs slightly between solvent exposed and buried networks. For solvent accessible networks, a decimal between 0 and 1 is randomly generated for each residue and compared to its decimal probability. If it is above that probability the residue is unprotonated, and if below it is protonated. This approach holds regardless of what the previous protonation state was. For solvent inaccessible networks, the decimal probabilities of all potential protonation configurations are put in a sequential order. A probability range for each configuration, S , is then defined as from P_L up to $P_L + P_C(R, S)$, where P_L is the sum of all configuration probabilities already considered and $P_C(R, S)$ is that of the current configuration. A decimal between 0 and 1 is then randomly generated, and the configuration is decided based on which range this number falls within. Any changes from the previous structure are then made, with hydrogen removed when necessary and DMD placing any new hydrogen on the appropriate heteroatoms. The structure is then ready for the next DMD simulation.

As the Titr-feature may add and remove hydrogen by exchange with implicit solvent, the energies of the structures before and after protonation state changes may not be directly comparable. Therefore, a correction to the DMD energy may be needed at the start of each DMD phase of the simulation. One approach would be to use a value for the solvation energy of a proton, but that can not be obtained directly from experiment and can only be determined by extrapolation.³⁸ Values that can be obtained for this (-264.3³⁹ and -265.9 kcal/mol^{38,40}) are large compared to the DMD energy changes associated with structural fluctuations (ca. 100 kcal/mol). Unmodified use of this proton solvation free energy would result in unphysical behavior – Titr-DMD would always deprotonate any residue. Appropriate scaling of the solvation energy is one solution. For this implementation of Titr-DMD an energy correction for each iteration is obtained instead based on the Propka pK_a of all residues with protonation states that deviate from the original structure. For each protonation state, take the following acid dissociation reaction



where $PRTN$ is the original protein and $PRTN^-$ is the new state. The free energy of this reaction can be written as

$$\Delta G_{deprot} = G(PRTN^-) + G(H^+) - G(PRTN)$$

Additionally, the K_a of this reaction is defined as

$$K_a = 10^{-\Delta G_{deprot}/RT}$$

Hence

$$G(PRTN^-) + G(H^+) = G(PRTN) - RT \ln(10^{-pK_a})$$

where $G(PRTN)$ is the uncorrected DMD energy and the left-hand side of the reaction is a corrected energy for a comparable system with the same chemical composition. For the protonation reaction, casting $PRTN$ as $PRTN^+$ and $PRTN^-$ as $PRTN$ in the original reaction gives the equation

$$G(PRTN^+) - G(H^+) = G(PRTN) + RT \ln(10^{-pK_a})$$

The energy associated with each protonation state change from the reference structure can therefore be written as $\pm RT \ln(10^{-pK_a})$, positive for protonation and negative for deprotonation. These are on the scale of 5-50 kcal/mol, consistent with DMD energy fluctuations. These terms are calculated for each iteration and summed with its DMD energy for the corrected energy.

Future development of Titr-DMD. The modularity of Titr-DMD allows for easy adaptation and refinement. Changes to the method do not require reparameterization of the force-field. Future developments of Propka or any other tool to calculate the instantaneous pK_a of a protein conformer can be exchanged to generate the probabilities of protonation state change and improve the quantitative accuracy of the feature. The Titr-feature could even be paired with another molecular mechanics method besides DMD, so long as it is in implicit solvent to retain simulation speed. Alternatives to the system-dependent solvent access cutoff are also of interest. One is to use the Propka buried percentage as a scalar probability of solvent accessibility rather than assign a sharp cutoff, while another is based on the solvent-excluded surface (SES) determined by reduced surface. This method defines the contour of the protein that can not be accessed by solvent by rolling a sphere with the van der Waals radius of the solvent (the ‘probe’) across the protein, avoiding the van der Waals radii of the other atoms.⁴¹ The solvent accessibility of any residue can be determined by measuring the distance of its titratable group to the nearest vertex of the water SES. If the vertex is within the van der Waals radius of the titratable group, it is solvent accessible. We are currently investigating these approaches for future developments.

Benchmark Systems. The systems considered for pK_a prediction have been studied extensively both experimentally and with other computational methods (Figure 2A-C). Hen egg-white lysozyme (HEWL) was used as it is a prototypical system for CpHMD benchmarking. The input structure of the protein was taken from the Protein Data Bank (PDB ID 1LZN).⁴² All solvent molecules were removed for the simulation – water, nitrogen trioxide, and the sodium ion. As HEWL only reports experimental pK_a for GLU, ASP, LYS, TYR, and a single HIS residue, both human thioredoxin (HTRX) and human muscle creatine kinase (HMCK) were simulated as well. HTRX brought in CYS and another HIS residue to the dataset alongside many more GLU and ASP. HMCK only added one CYS residue to the dataset, but was included as it is one of the largest proteins with an experimentally identified amino acid pK_a at 381 residues (compared to 105 residues for HTRX and 129 for HEWL). The initial structure used for HTRX was PDB ID 1ERT,⁴³ with all water molecules removed and the rotamers labeled ‘A’ used when more than one was recorded. As it is unclear whether the 320-331 loop of HMCK is unstructured or an alpha helix, two structures were used. The unstructured case was based on the A chain of PDB ID 1U6R,⁴⁴ mutated back to the WT sequence with the substrate ADP, inhibitor (diaminomethyl-methyl-amino)-acetic acid, all water, nitrogen trioxide, and magnesium ions removed. The alpha loop struc-

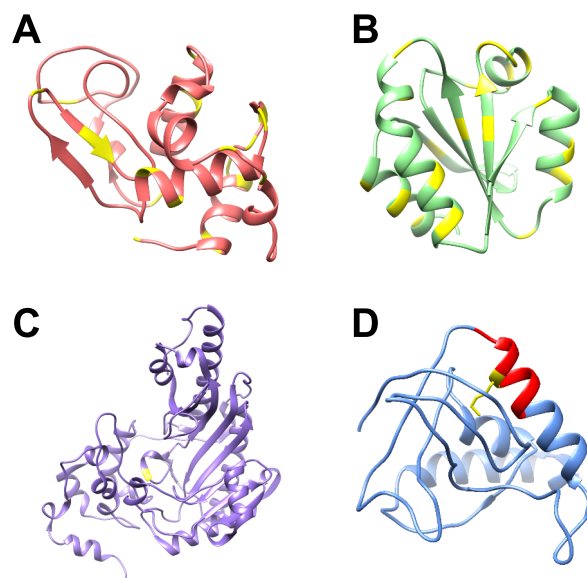


Figure 2: Ribbon diagrams of protein test systems for Titr-DMD benchmarking: HEWL (A), HTRX (B), HMCK (C), and SNase mutant V66K (D). The residues whose pK_a 's are considered and compared to experiment are highlighted in yellow. In the case of the SNase mutant, this is the buried LYS66 residue. The alpha helical loop to which it belongs and that unravels is shown in red.

ture was the same except the 320-331 loop was replaced with the 321-332 loop of the A-chain from PDB ID 3B6R.⁴⁵ All experimental reference pK_a were drawn from the PKAD database.⁴⁶ The pK_a values used ultimately come from Bartik et al.⁴⁷ and Webb et al.⁴⁸ for HEWL, from Forman-Kay et al.⁴⁹ and Qin et al.⁵⁰ for HTRX, and Wang et al.⁵¹ for HMCK. The pK_a predictions from our simulations measure error and deviations to the average of these datasets for each residue with more than one reported value.

The system used to assess pH -conformational coupling was Staphylococcal nuclease mutant V66K, a well characterized system (Figure 2D). Experimental information about protein conformational dynamics, including in the context of pH change, is difficult to obtain. As discussed in the introduction, the study of SNase mutants is a rare example of this being done. A combination of NMR, CD, and titration suggests that the protonation of LYS66 is concurrent with and may be coupled to the unraveling of the first loop of the alpha helix on which it is located.^{32,52-54} The V66K mutant was selected as it demonstrates an extreme pK_a shift of 10.5 down to 5.7 – which alongside the conformational coupling is a real challenge for any CpHMD method. The structure used was PDB ID 2SNM⁵⁵ with thymidine-3',5'-diphosphate, water molecules, and the calcium ion removed.

Titr-DMD settings. Benchmarking simulations differ slightly between those done to estimate pK_a values and those that assess pH -conformational coupling. The pH -conformational coupling simulations were longer and hotter to achieve the necessary sampling. DMD simulations without the Titr-feature were also run for the pH -conformation coupling system as a control – to make sure conformational changes are pH dependent. The pK_a estimating simulations were run for 2,000,000 DMD timesteps (roughly 100 ns) at 50 K (note that temperature in DMD is defined specifically, and does not di-

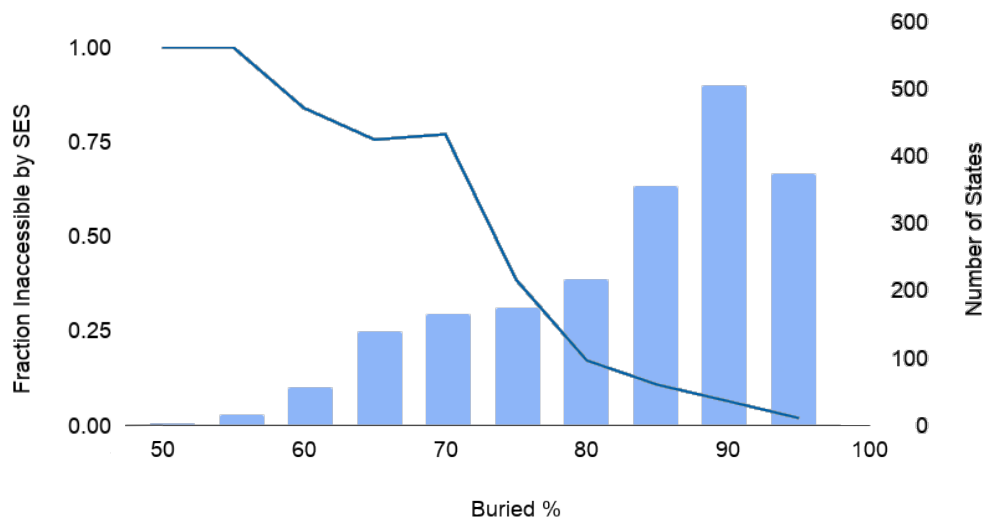


Figure 3: Comparison of the Propka buried percentage to solvent accessibility according to the reduced surface SES. The dark blue line is the fraction of states that are solvent inaccessible according to the SES, where 1 is totally inaccessible and 0 is entirely accessible (left axis). The light blue histogram is the number of states in that bin (right axis). States are binned in units of 5 buried percentage points. Note that most states below 65-70% buried are solvent inaccessible according to the SES and that those below 55-60% buried are entirely inaccessible according to the SES.

rectly correspond to the physical temperature).²⁹ A high heat exchange of 10.0 was used for thermal stability because Titr-DMD consists of many short DMD simulations – a more typical, low value has a destabilizing effect. As discussed with the description of the method, a standard protonation contact distance of 3.5 Å was used, as well as the standard protonation state reassessment frequency of 200 steps. The solvent access cutoff was 75%, which will be discussed in more detail in the next paragraph. The *pH*-conformation coupling simulations were run for a longer 4,000,000 DMD timesteps (roughly 200 ns) with solvent access cutoff values of 65% and 45% ultimately selected and a temperature of 150K for increased mobility. The other settings were the same as for the *pK_a* prediction. The DMD control simulations without the Titr-feature were run for the same time and temperature as the *pH*-conformational coupling simulations.

The exact value of the solvent access cutoff is system dependent and requires special attention/calibration. A cutoff of 75% was originally selected for all of the simulations conducted here. A Propka calculation on the initial structure for each system yielded buried values above ~75% for only the entirely buried residues and those nestled in internal folds, while the external surface residues were all well below this percentage. Over the course of the Titr-DMD simulations, only 2 of the 40 residues with experimentally available *pK_a* in the benchmark set stayed consistently buried (ASP26 in HTRX and CYS282 in HMCK), so these simulations were ultimately not too sensitive to the choice of solvent buried cutoff. This choice was, however, very critical for simulations of *pH*-conformational coupling, as they involved a study of whether the protonation state of a deeply buried residue (LYS66 in a staphylococcal nuclease mutant V66K) is coupled to the dynamics of the protein. In this case, we ran full simulations at a series of different solvent access cutoff (25%, 35%, 45%, 55%, and 65%) and determined the most physical cutoff based on a comparison to the reduced surface SES. LYS66 was then defined as solvent accessible if its amine group is within its van der Waals radius of three vertices (one face) of the SES. The comparison to the solvent access cutoff was done for a 20

ns test Titr-DMD simulation of SNase V66K with a solvent access cutoff of 75%. The solvent accessibility was then calculated for each iteration with a SES generated by Chimera (v 1.13.1).⁵⁶ The iterations were binned based on their Propka predicted percent buried, and the percent of states deemed to be solvent accessible was calculated for each bin (Figure 3). The results show that for SNase V66K there is a threshold around 65-75% buried where LYS66 is generally buried above that point and not buried below that point. Structures do not, however, become entirely solvent accessible until below 55%. It is important to note that such a low Propka buried % is rare for LYS66 in our short test simulation. We therefore selected for analysis the SNase simulations with solvent access cutoffs of 65% and 45%, one around the inflection point (in Figure 2) and one where LYS66 is only solvent accessible when it is assured based on our SES test. The results of the other cutoffs are reported in the supporting information (Figure S1, Tables S1-S3).

A total of 45 Titr-DMD and 4 DMD simulations were performed for benchmarking. Simulations were done for HEWL at *pH* 3, 5, 7, and 9, for HTRX at *pH* 3, 5, and 7, and for HMCK both with the unstructured and alpha helical 320-331 loop at *pH* 9. The *pH* values were selected to straddle the *pK_a* of residues with experimentally reported values. Simulations were run for SNase at *pH* 4.6, 5.7, and 7. These values are below, at, and above the experimental *pK_a* of the LYS66 residue and its coupled dynamic behavior. All are above the denaturing point of the protein. Three replicates were performed for each system and *pH*. The four DMD simulations were run for SNase to provide a point of comparison. Two were run with LYS66 permanently deprotonated and two with it permanently protonated.

Convergence of the Titr-DMD simulations was attained according to a pair of metrics. This is comprised of the backbone RMSD and the corrected Titr-DMD energy (Figure 4). The RMSD was calculated with the initial structure as the reference and with respect to the alpha carbon and amide nitrogen, carbon, and oxygen of each amino acid. All trajectories come to oscillate around fixed values, indicating convergence.

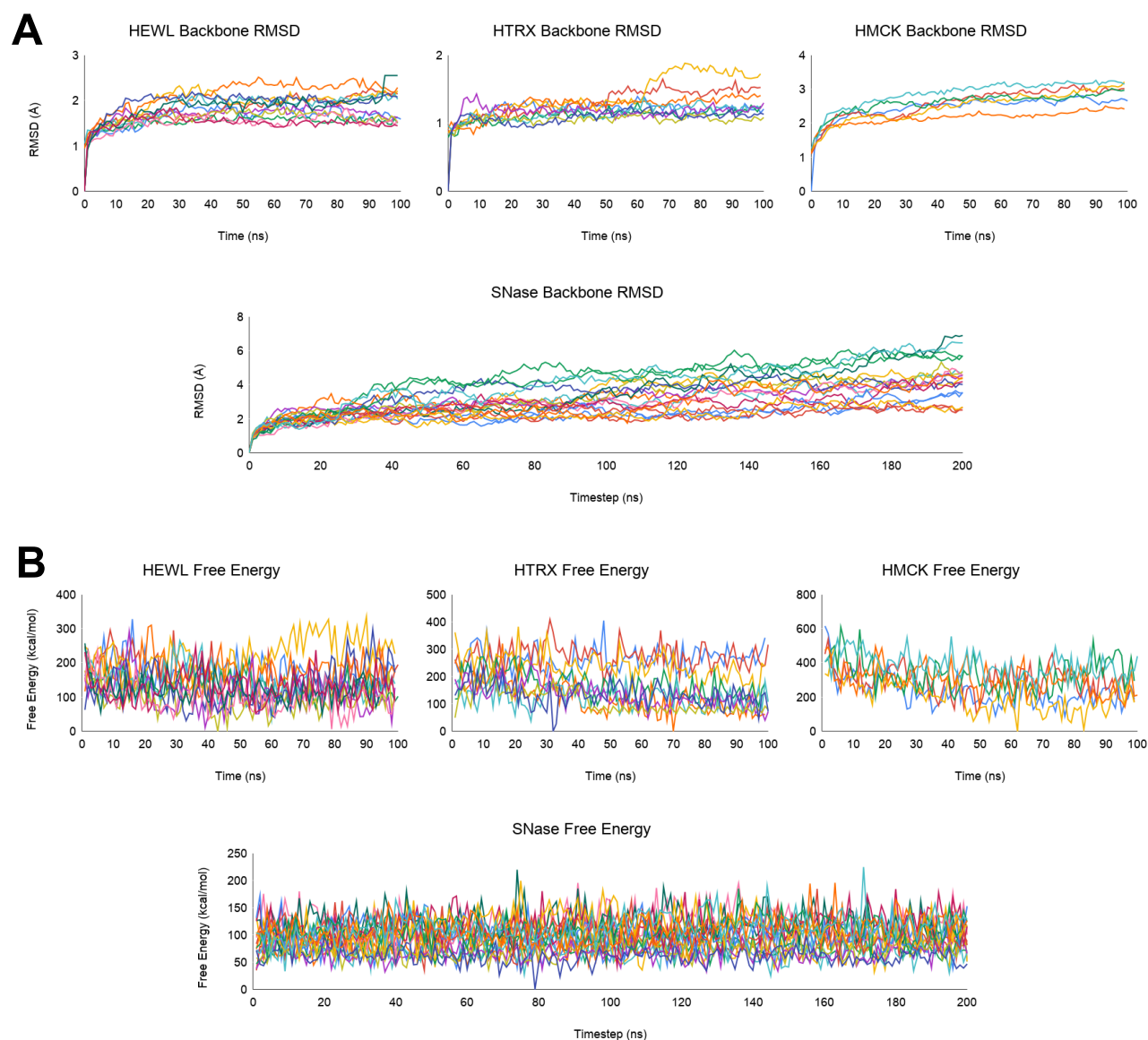


Figure 4: Convergence of Titr-DMD simulations tracked by (A) the backbone RMSD and (B) corrected DMD free energy. Note that by both metrics the results come to oscillate around fixed values by the end of the simulations.

Results and Discussion

Titr-DMD offers rapid sampling on limited resources. The combination of DMD and Propka in an implicit solvent makes it a fast and affordable method. We assessed the scaling of Titr-DMD through 1000 step (5 protonation assessments, about 50 ps) simulations of HEWL, HTRX, and HMCK executed with 1, 2, 4, 8, and 16 processors both with and without the Titr-feature. All simulations were run on the same node sequentially during a single submission to reduce the impact of the variability of other demands on the supercomputing cluster. Simulations were performed on AMD Opteron 2380 (2.5 GHz) cores on Hoffman2 at UCLA IDRE. This process was replicated five times, with the average of these results taken (Figure 5). Titr-DMD scales roughly linearly with the number of residues, and scales favorably out to four processors, with additional resources giving diminished returns. The Titr-feature does modestly increase the computational expense of DMD simulations, with the increase in relative runtime over base DMD growing some with the number of processors used.

This largely derives from the need to initialize many short DMD simulations. However, Titr-DMD still runs quite well on limited resources; the CPU time for the four processor tests scales up to 500-1300 CPU hours (or 3-5.5 CPU hours per residue) to reach a 1 ms simulation.

With a couple exceptions, our Titr-DMD method successfully recaptured the experimental pK_a of the test system residues. We calculated the average RMSE between the predicted and experimental values both by type of amino acid and by protein test system (Tables 1-2). The pK_a can be calculated two ways from Titr-DMD, therefore we calculated two average RMSE for each case. Propka pK_a is simply the average of the Propka predicted values from each timestep. The DMD pK_a for a residue is the natural logarithm of the fraction of timesteps in which the residue is protonated. That fraction is analogous to the K_a : the relative concentration of the protonated form of the residue. For solvent exposed residues (those that can freely change protonation state just based on their instantaneous pK_a) these two pK_a predictions should converge to the same values with appropriate Monte-Carlo sampling. The

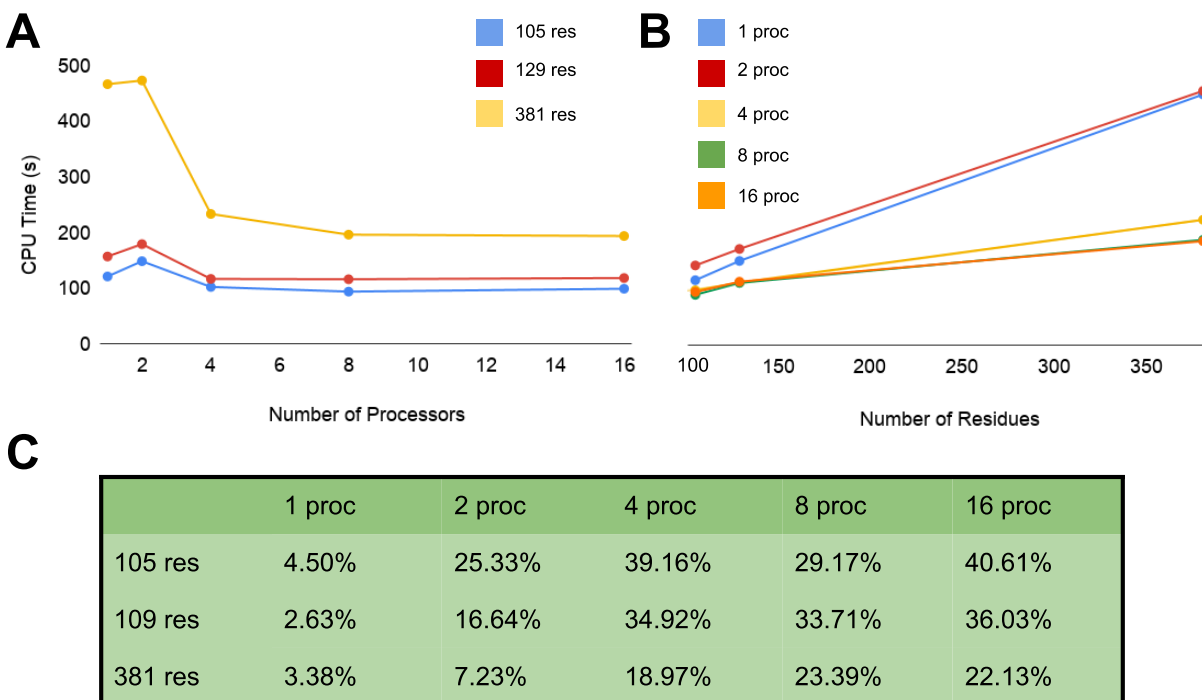


Figure 5: Computational resource scaling benchmark of Titr-DMD, plotted by (A) the number of processors and (B) the number of residues. Note the linear scaling with number of residues and that good performance is reached with four processors. (C) The percent increase of time for Titr-DMD over unmodified DMD. Note that the increase is relatively small and only becomes significant with many processors as the time DMD takes shortens.

results show that indeed the average RMSE are in good agreement between the two methods for each system, with generally small values around or below 1. The only exceptions are for aspartate and cysteine residues. In the case of aspartate it appears that Propka does poorly specifically with residues that have especially depressed values below 2. Cysteine, on the other hand, is handled uniformly poorly by Propka. This may have to do with the fact that both residues are partially buried and one participates in a disulfide bond (which could complicate the Propka prediction and is handled in an ad-hoc manner by DMD). Furthermore, our test set only includes two cysteine residues as experimentally obtained values for this amino acid are rare; the pK_a predictions for these particular residues could simply be anomalously poor. A different instantaneous pK_a prediction method than Propka may improve accuracy for these specific residues when necessary for a simulation.

Table 1: Titr-DMD pK_a RMSE by amino acid compared to experimental values. Each is calculated relative to an aggregate dataset compiled from all considered experimental studies. HEWL, HTRX, and HMCK are all included.

Amino Acid	DMD RMSE	Propka RMSE
ASP	1.49	1.44
GLU	0.47	0.63
HIS	0.53	0.47
LYS	0.76	0.81
TYR	0.67	0.52
CYS	2.28	3.87

Titr-DMD predictions of pK_a values are competitive with more expensive CpHMD methods. We compare our method on a truncated set of residues that was also assessed by the explicit solvent Vila-Viçosa et al.²⁸ and the Goh et al.²³ replica exchange CpHMD methods, and the implicit solvent implementation of the Wallace et al.²⁷ replica exchange CpHMD method. This set includes mostly aspartate and glutamate residues as well as one histidine residue. For this set the Wallace method obtains an RMSE of 0.89 while the Goh method obtains 0.83 and the Vila-Viçosa method obtains 0.83. Our RMSE of 1.47 or 1.45 (for the DMD and Propka pK_a respectively) is reasonable, as the truncated set of HEWL residues heavily features low- pK_a aspartate residues, with which our method does worse, and entirely excludes lysine and tyrosine. The RMSE for other residues besides aspartate and cysteine are on par with the more expensive methods.

Table 2: Titr-DMD pK_a RMSE by protein system compared to experimental values. HEWL* consists of the ASP and GLU residues that are considered in other CpHMD method benchmarks and is comparable to them, while HEWL includes LYS, TYR, and HIS residues as well.

System	DMD RMSE	Propka RMSE
HEWL	1.30	1.27
HEWL*	1.47	1.45
HTRX	1.07	0.93
HMCK		5.66

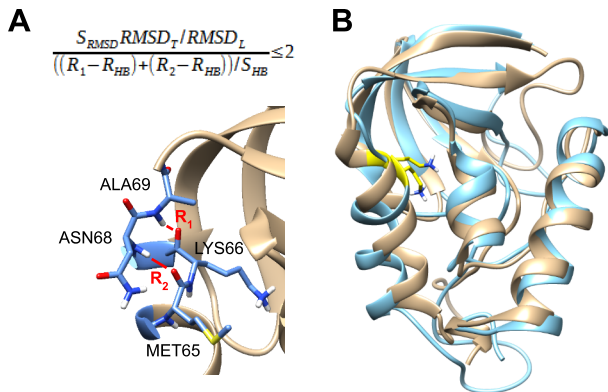


Figure 6: (A) Criterion for an unraveled 65-69 loop structure in our SNase simulations. This compares the RMSD of the loop ($RMSD_L$) to the RMSD of the full protein ($RMSD_T$) and compares the distances of important hydrogen bonding contacts (R_1 , R_2) to standard values (R_{HB}) to determine structures where the conformation of the loop varies significantly from the original structure. We give the values of the other variables in the main text. (B) Example of a SNase conformation with an unraveled 65-69 loop by our criterion (light blue) overlaid on a structure where it is not unraveled (tan). LYS66 is colored yellow here.

Titri-DMD holds promise for the study of the effect of solution pH on protein structure. Simulations of SNase V66K are qualitatively consistent with rare, experimentally studied dynamics. With the Titri-feature, we observe partial unraveling of the first turn of the alpha helix on which K66 is localized on (residues 65-69), which is not apparent in DMD without titration (Table 3). Unraveling is only observed in 0.002-0.015% of structures in base DMD, while Titri-DMD simulations show it occurs in 3-8% of structures. We define an unraveled state as one where the ALA69-LYS66 and ASN68-MET65 hydrogen bonds are broken or breaking and the backbone RMSD of the loop is large relative to that of the full protein, indicative of significant, localized structural change (Figure 6). The criterion is

$$\frac{S_{RMSD} RMSD_T / RMSD_L}{((R_1 - R_{HB}) + (R_2 - R_{HB})) / S_{HB}} \leq 2$$

where $RMSD_T$ is for the total protein and $RMSD_L$ is for the loop (residues 65-69), R_1 and R_2 are the backbone amide H to carbonyl O distances in Å of ALA69-LYS66 and ASN68-MET65 respectively, S_{RMSD} is 2, R_{HB} is 2.5 Å (for a long hydrogen bond length), and S_{HB} is 2 Å. We only consider structures where the ALA69-LYS66 and ASN68-MET65 backbone hydrogen bond distances are both at least 3 Å. While unraveling according to our criterion occurs in 3-8% of all states at the appropriate pH , it is not typically sustained for longer than about 1 ns at any one time. We surmise that our simulations do not have enough sampling to capture sustained loop unraveling, but do show the rare events that could lead to it.

Table 3: Frequency of SNase mutant V66K alpha helical loop 65-69 unraveling over the course of Titri-DMD (upper) and DMD (lower) simulations. Note that the frequency is much higher in the Titri-DMD simulations. The highest frequency that occurs at the experimental pK_a of LYS66 (5.7) is when the solvent access cutoff is 45%.

Simulation	pH 4.6	pH 5.7	pH 7
45% cutoff	5.68%	7.06%	4.68%
65% cutoff	3.84%	5.64%	7.93%
	Prot	Deprot	
Base DMD	0.002%	0.015%	

Protonation and deprotonation of LYS66 is coupled with loop unraveling according to Titri-DMD. At pH 5.7, the percentage of unraveled states is significantly higher around LYS66 protonation state changes than the total simulation average (Table 4). Moreover, few events at pH 5.7 occur without contemporaneous unraveling. The coupling we observe in our simulations is thus consistent with the experimental hypothesis.³²

Table 4: Frequency of unraveling of the SNase mutant 65-69 loop around LYS66 protonation and deprotonation events. ‘Near event’ refers to the percentage of structures within 25 timesteps (before and after) of an event that are unraveled. This value is roughly on par with the total simulation average except at pH 5.7, particularly during the simulation with a 45% solvent access cutoff. ‘By event’ refers to the percent of events that have at least one unraveled structure within 25 timesteps. Again, note that the pH 5.7 simulations show high coupling where protonation state changes nearly always occur alongside some contemporaneous unraveling.

Near Event	pH 4.6	pH 5.7	pH 7
45% cutoff	1.11%	30.43%	0.54%
65% cutoff	3.20%	9.45%	10.97%
By Event			
45% cutoff	25%	85%	20%
65% cutoff	20%	80%	29%

Titri-DMD dynamics can predict the pH at which loop unraveling occurs. The Propka predicted pK_a value of LYS66 is uniformly higher than the experimental 5.7, at an average of 7-8, but still shows a qualitatively correct large drop from the solution value of 10.5 (Table 5). However, the DMD pK_a is gen-

erally lower, representing the frequent solvent inaccessibility of the residue. With the solvent access cutoff tuned to 45% it even comes close to the experimental finding. At this cutoff, unraveling is most common in the pH 5.7 simulations and nearly all protonation state changes occur alongside some unraveling. Titr-DMD can qualitatively model coupling between pH and protein structure, and when well calibrated can do so with more quantitative accuracy.

Table 5: Titr-DMD predicted pK_a for LYS66 in the SNase mutant. These values are averages across all replicate simulations. All of these are above the experimental value, though still significantly shifted down from the solution value of 10.5, except the DMD pK_a value for the 45% solvent access cutoff simulation. This reflects the typically solvent shielded environment of LYS66 modeled through DMD dynamics that Propka underestimates on its own.

Simulation	DMD	Propka
45% cutoff	5.79	7.80
65% cutoff	7.04	7.96

Conclusions

In this paper we demonstrate Titr-DMD as an effective new method to study pH coupled protein dynamics. The challenges that face any CpHMD method are appropriate conformational and protonation state sampling, accuracy of protonation state changes, and whether the generated conformational ensemble is physically meaningful. Titr-DMD offers great sampling on just a few processors through atomic collision event calculations, implicit solvation, and semi-empirical pK_a prediction with Propka. Our method obtains reasonably accurate pK_a predictions for its computational expense. Titr-DMD was successfully benchmarked on the partial unraveling of SNase mutant V66K: one of the few experimentally studied pH coupled conformational changes. Titr-DMD generates a conformational ensemble consistent with experiment, and this ensemble even reflects the experimental pH value of the conformational change. Our method is also modular to further improve sampling and accurate assignment of protonation states. Titr-DMD stands as a promising method to address questions of pH dynamics in industrial catalysis and medicine.

ASSOCIATED CONTENT

Supporting Information is available free of charge via the Internet at <http://pubs.acs.org>.

AUTHOR INFORMATION

Corresponding Author

*E-mail: ana@chem.ucla.edu. Phone: +1 310 8253769

Funding Sources

Financial support comes from the NSF CHE-1903808 grant to A.N.A., and from the Passan Foundation and US National Institutes of Health grant R35 GM134864 to N.V.D. We also acknowledge UCLA-IDRE and XSEDE for providing computational resources.

Notes

We declare no competing financial interest.

ACKNOWLEDGMENT

We thank the Institute for Digital Research and Education at UCLA and the Extreme Science and Engineering Discovery Environment for supercomputer time. We thank Matthew Hennefarth for advice on integration of the Titr-feature with DMD and a new implementation of DMD. We thank Prof. Feng Ding for advice on the heat exchange parameter of DMD.

ABBREVIATIONS

SNase, staphylococcal nuclease; HTRX, human thioredoxin; HEWL, hen egg-white lysozyme; HMCK, human muscle creatine kinase; SES; solvent-excluded surface.

REFERENCES

- (1) Dumorné, K.; Córdova, D. C.; Astorga-Eló, M.; Renganathan, P. Extremozymes: A Potential Source for Industrial Applications. *J Microbiol Biotechnol* **2017**, *27* (4), 649–659.
- (2) Sarmiento, F.; Peralta, R.; Blamey, J. M. Cold and Hot Extremozymes: Industrial Relevance and Current Trends. *Front. Bioeng. Biotechnol.* **2015**, *3*, 148.
- (3) Chen, G.-Q.; Jiang, X.-R. Next Generation Industrial Biotechnology Based on Extremophilic Bacteria. *Curr. Opin. Biotechnol.* **2018**, *50*, 94–100.
- (4) Fernandes, P. Enzymes in Food and Feed Industries: Where Tradition Meets Innovation. In *Biocatalysis*; Springer, 2019; pp 233–253.
- (5) Rivinoja, A.; Pujol, F. M.; Hassinen, A.; Kellokumpu, S. Golgi PH, Its Regulation and Roles in Human Disease. *Ann. Med.* **2012**, *44* (6), 542–554.
- (6) Webb, B. A.; Chimenti, M.; Jacobson, M. P.; Barber, D. L. Dysregulated PH: A Perfect Storm for Cancer Progression. *Nat. Rev. Cancer* **2011**, *11* (9), 671–677.
- (7) Fang, B.; Wang, D.; Huang, M.; Yu, G.; Li, H. Hypothesis on the Relationship between the Change in Intracellular PH and Incidence of Sporadic Alzheimer's Disease or Vascular Dementia. *Int. J. Neurosci.* **2010**, *120* (9), 591–595.
- (8) Dokholyan, N. V. Experimentally-Driven Protein Structure Modeling. *J. Proteomics* **2020**, *220*, 103777.
- (9) Fogolari, F.; Brigo, A.; Molinari, H. The Poisson–Boltzmann Equation for Biomolecular Electrostatics: A Tool for Structural Biology. *J. Mol. Recognit.* **2002**, *15* (6), 377–392.
- (10) Bashford, D.; Gerwert, K. Electrostatic Calculations of the PKa Values of Ionizable Groups in Bacteriorhodopsin. *J. Mol. Biol.* **1992**, *224* (2), 473–486.
- (11) Onufriev, A. V.; Case, D. A. Generalized Born Implicit Solvent Models for Biomolecules. *Annu. Rev. Biophys.* **2019**, *48*, 275–296.
- (12) Madura, J. D.; Briggs, J. M.; Wade, R. C.; Davis, M. E.; Luty, B. A.; Ilin, A.; Antosiewicz, J.; Gilson, M. K.; Bagheri, B.; Scott, L. R. Electrostatics and Diffusion of Molecules in Solution: Simulations with the University of Houston Brownian Dynamics Program. *Comput. Phys. Commun.* **1995**, *91* (1–3), 57–95.
- (13) Anandakrishnan, R.; Aguilar, B.; Onufriev, A. V. H++ 3.0: Automating p K Prediction and the Preparation of Biomolecular Structures for Atomistic Molecular Modeling and Simulations. *Nucleic Acids Res.* **2012**, *40* (W1), W537–W541.
- (14) Olsson, M. H. M.; Søndergaard, C. R.; Rostkowski, M.; Jensen, J. H. PROPKA3: Consistent Treatment of Internal and Surface Residues in Empirical p K a Predictions. *J. Chem. Theory Comput.* **2011**, *7* (2), 525–537.
- (15) Søndergaard, C. R.; Olsson, M. H. M.; Rostkowski, M.; Jensen, J. H. Improved Treatment of Ligands and Coupling Effects in Empirical Calculation and Rationalization of p K a Values. *J. Chem. Theory Comput.* **2011**, *7* (7), 2284–2295.
- (16) Bürgi, R.; Kollman, P. A.; van Gunsteren, W. F. Simulating Proteins at Constant PH: An Approach Combining Molecular Dynamics and Monte Carlo Simulation. *Proteins Struct. Funct. Bioinforma.* **2002**, *47* (4), 469–480.
- (17) Mongan, J.; Case, D. A.; McCAMMON, J. A. Constant PH Molecular Dynamics in Generalized Born Implicit Solvent. *J. Comput. Chem.* **2004**, *25* (16), 2038–2048.
- (18) Barroso da Silva, F. L.; MacKernan, D. Benchmarking a Fast Proton Titration Scheme in Implicit Solvent for Biomolecular Simulations. *J. Chem. Theory Comput.* **2017**, *13* (6), 2915–2929.
- (19) Harris, R. C.; Liu, R.; Shen, J. Predicting Reactive Cysteines with Implicit-Solvent-Based Continuous Constant PH Molecular Dynamics in Amber. *J. Chem. Theory Comput.* **2020**, *16* (6), 3689–3698.
- (20) Lee, M. S.; Salsbury Jr, F. R.; Brooks III, C. L. Constant-pH Molecular Dynamics Using Continuous Titration Coordinates. *Proteins Struct. Funct. Bioinforma.* **2004**, *56* (4), 738–752.

- (21) Jorgensen, W. L.; Chandrasekhar, J.; Madura, J. D.; Impey, R. W.; Klein, M. L. Comparison of Simple Potential Functions for Simulating Liquid Water. *J. Chem. Phys.* **1983**, 79 (2), 926–935.
- (22) Tidor, B. Simulated Annealing on Free Energy Surfaces by a Combined Molecular Dynamics and Monte Carlo Approach. *J. Phys. Chem.* **1993**, 97 (5), 1069–1073.
- (23) Goh, G. B.; Hulbert, B. S.; Zhou, H.; Brooks III, C. L. Constant PH Molecular Dynamics of Proteins in Explicit Solvent with Proton Tautomerism. *Proteins Struct. Funct. Bioinforma.* **2014**, 82 (7), 1319–1331.
- (24) Chen, Y.; Roux, B. Constant-PH Hybrid Nonequilibrium Molecular Dynamics–Monte Carlo Simulation Method. *J. Chem. Theory Comput.* **2015**, 11 (8), 3919–3931.
- (25) Huang, Y.; Harris, R. C.; Shen, J. Generalized Born Based Continuous Constant PH Molecular Dynamics in AMBER: Implementation, Benchmarking and Analysis. *J. Chem. Inf. Model.* **2018**, 58 (7), 1372–1383.
- (26) Harris, R. C.; Shen, J. GPU-Accelerated Implementation of Continuous Constant PH Molecular Dynamics in Amber: P K a Predictions with Single-PH Simulations. *J. Chem. Inf. Model.* **2019**, 59 (11), 4821–4832.
- (27) Wallace, J. A.; Shen, J. K. Continuous Constant PH Molecular Dynamics in Explicit Solvent with PH-Based Replica Exchange. *J. Chem. Theory Comput.* **2011**, 7 (8), 2617–2629.
- (28) Vila-Viçosa, D.; Reis, P. B. P. S.; Baptista, A. M.; Oostenbrink, C.; Machuqueiro, M. A PH Replica Exchange Scheme in the Stochastic Titration Constant-PH MD Method. *J. Chem. Theory Comput.* **2019**, 15 (5), 3108–3116.
- (29) Ding, F.; Tsao, D.; Nie, H.; Dokholyan, N. V. Ab Initio Folding of Proteins with All-Atom Discrete Molecular Dynamics. *Structure* **2008**, 16 (7), 1010–1018.
- (30) Proctor, E. A.; Ding, F.; Dokholyan, N. V. Discrete Molecular Dynamics. *Wiley Interdiscip. Rev. Comput. Mol. Sci.* **2011**, 1 (1), 80–92.
- (31) Shirvanyants, D.; Ding, F.; Tsao, D.; Ramachandran, S.; Dokholyan, N. V. Discrete Molecular Dynamics: An Efficient and Versatile Simulation Method for Fine Protein Characterization. *J. Phys. Chem. B* **2012**, 116 (29), 8375–8382.
- (32) Isom, D. G.; Castañeda, C. A.; Cannon, B. R. Large Shifts in PKa Values of Lysine Residues Buried inside a Protein. *Proc. Natl. Acad. Sci.* **2011**, 108 (13), 5260–5265.
- (33) Vila-Viçosa, D.; Campos, S. R. R.; Baptista, A. M.; Machuqueiro, M. Reversibility of Prion Misfolding: Insights from Constant-PH Molecular Dynamics Simulations. *J. Phys. Chem. B* **2012**, 116 (30), 8812–8821.
- (34) Shi, C.; Wallace, J. A.; Shen, J. K. Thermodynamic Coupling of Protonation and Conformational Equilibria in Proteins: Theory and Simulation. *Biophys. J.* **2012**, 102 (7), 1590–1597.
- (35) Peck, M. T.; Ortega, G.; De Luca-Johnson, J. N.; Schlessman, J. L.; Robinson, A. C.; García-Moreno E, B. Local Backbone Flexibility as a Determinant of the Apparent p K a Values of Buried Ionizable Groups in Proteins. *Biochemistry* **2017**, 56 (40), 5338–5346.
- (36) Schramm, V. L.; Schwartz, S. D. Promoting Vibrations and the Function of Enzymes. Emerging Theoretical and Experimental Convergence. *Biochemistry* **2018**, 57 (24), 3299–3308.
- (37) Fang, C.; Frontiera, R. R.; Tran, R.; Mathies, R. A. Mapping GFP Structure Evolution during Proton Transfer with Femtosecond Raman Spectroscopy. *Nature* **2009**, 462 (7270), 200–204.
- (38) Kelly, C. P.; Cramer, C. J.; Truhlar, D. G. Aqueous Solvation Free Energies of Ions and Ion–Water Clusters Based on an Accurate Value for the Absolute Aqueous Solvation Free Energy of the Proton. *J. Phys. Chem. B* **2006**, 110 (32), 16066–16081.
- (39) Zhan, C.-G.; Dixon, D. A. Absolute Hydration Free Energy of the Proton from First-Principles Electronic Structure Calculations. *J. Phys. Chem. A* **2001**, 105 (51), 11534–11540.
- (40) Tissandier, M. D.; Cowen, K. A.; Feng, W. Y.; Gundlach, E.; Cohen, M. H.; Earhart, A. D.; Coe, J. V; Tuttle, T. R. The Proton’s Absolute Aqueous Enthalpy and Gibbs Free Energy of Solvation from Cluster-Ion Solvation Data. *J. Phys. Chem. A* **1998**, 102 (40), 7787–7794.

- (41) Sanner, M. F.; Olson, A. J.; Spehner, J. Reduced Surface: An Efficient Way to Compute Molecular Surfaces. *Biopolymers* **1996**, *38* (3), 305–320.
- (42) Bon, C.; Lehmann, M. S.; Wilkinson, C. Quasi-Laue Neutron-Diffraction Study of the Water Arrangement in Crystals of Triclinic Hen Egg-White Lysozyme. *Acta Crystallogr. Sect. D Biol. Crystallogr.* **1999**, *55* (5), 978–987.
- (43) Weichsel, A.; Gasdaska, J. R.; Powis, G.; Montfort, W. R. Crystal Structures of Reduced, Oxidized, and Mutated Human Thioredoxins: Evidence for a Regulatory Homodimer. *Structure* **1996**, *4* (6), 735–751.
- (44) Ohren, J. F.; Kundracik, M. L.; Borders, C. L.; Edmiston, P.; Viola, R. E. Structural Asymmetry and Intersubunit Communication in Muscle Creatine Kinase. *Acta Crystallogr. Sect. D Biol. Crystallogr.* **2007**, *63* (3), 381–389.
- (45) Bong, S. M.; Moon, J. H.; Nam, K. H.; Lee, K. S.; Chi, Y. M.; Hwang, K. Y. Structural Studies of Human Brain-Type Creatine Kinase Complexed with the ADP–Mg²⁺–NO₃–Creatine Transition-State Analogue Complex. *FEBS Lett.* **2008**, *582* (28), 3959–3965.
- (46) Pahari, S.; Sun, L.; Alexov, E. PKAD: A Database of Experimentally Measured PKa Values of Ionizable Groups in Proteins. *Database* **2019**, 2019.
- (47) Bartik, K.; Redfield, C.; Dobson, C. M. Measurement of the Individual PKa Values of Acidic Residues of Hen and Turkey Lysozymes by Two-Dimensional ¹H NMR. *Biophys. J.* **1994**, *66* (4), 1180–1184.
- (48) Webb, H.; Tynan-Connolly, B. M.; Lee, G. M.; Farrell, D.; O'Meara, F.; Søndergaard, C. R.; Teilum, K.; Hewage, C.; McIntosh, L. P.; Nielsen, J. E. Remeasuring HEWL PKa Values by NMR Spectroscopy: Methods, Analysis, Accuracy, and Implications for Theoretical PKa Calculations. *Proteins Struct. Funct. Bioinforma.* **2011**, *79* (3), 685–702.
- (49) Forman-Kay, J. D.; Clore, G. M.; Gronenborn, A. M. Relationship between Electrostatics and Redox Function in Human Thioredoxin: Characterization of PH Titration Shifts Using Two-Dimensional Homo- and Heteronuclear NMR. *Biochemistry* **1992**, *31* (13), 3442–3452.
- (50) Qin, J.; Clore, G. M.; Gronenborn, A. M. Ionization Equilibria for Side-Chain Carboxyl Groups in Oxidized and Reduced Human Thioredoxin and in the Complex with Its Target Peptide from the Transcription Factor NFκB. *Biochemistry* **1996**, *35* (1), 7–13.
- (51) Wang, P.-F.; McLeish, M. J.; Kneen, M. M.; Lee, G.; Kenyon, G. L. An Unusually Low p K a for Cys282 in the Active Site of Human Muscle Creatine Kinase. *Biochemistry* **2001**, *40* (39), 11698–11705.
- (52) Takayama, Y.; Castaneda, C. A.; Chimenti, M.; García-Moreno, B.; Iwahara, J. Direct Evidence for Deprotonation of a Lysine Side Chain Buried in the Hydrophobic Core of a Protein. *J. Am. Chem. Soc.* **2008**, *130* (21), 6714–6715.
- (53) Karp, D. A.; Stahley, M. R.; García-Moreno, E. B. Conformational Consequences of Ionization of Lys, Asp, and Glu Buried at Position 66 in Staphylococcal Nuclease. *Biochemistry* **2010**, *49* (19), 4138–4146.
- (54) Chimenti, M. S.; Khangulov, V. S.; Robinson, A. C.; Heroux, A.; Majumdar, A.; Schlessman, J. L.; García-Moreno, B. Structural Reorganization Triggered by Charging of Lys Residues in the Hydrophobic Interior of a Protein. *Structure* **2012**, *20* (6), 1071–1085.
- (55) Stites, W. E.; Gittis, A. G.; Lattman, E. E.; Shortle, D. In a Staphylococcal Nuclease Mutant the Side-Chain of a Lysine Replacing Valine 66 Is Fully Buried in the Hydrophobic Core. *J. Mol. Biol.* **1991**, *221* (1), 7–14.
- (56) Pettersen, E. F.; Goddard, T. D.; Huang, C. C.; Couch, G. S.; Greenblatt, D. M.; Meng, E. C.; Ferrin, T. E. UCSF Chimera—a Visualization System for Exploratory Research and Analysis. *J. Comput. Chem.* **2004**, *25* (13), 1605–1612.